HSM2023-00013

MODELING OF CUTTING TEMPERATURE IN SCREW WHIRLING MILLING DURING THE TWO CUTTING STAGES

Chao Liu[1, 2, *], Shaofu Huang[1, 2], Yan He[3], Zunpeng Huang[1], Zidong Yang[1]

[1] Anhui University of Science and Technology, College of Mechanical Engineering, Huainan, China

[2] Anhui University of Science and Technology, Institute of Environment-friendly Materials and Occupational Health, Wuhu, China

[3] Chongqing University, State Key Laboratory of Mechanical Transmission, Chongqing, China

*Corresponding author; e-mail: liuchaomech@163.com

Abstract

Temperature analysis in the manufacturing phase of the product is necessary for improving the operational performance of the workpiece. In screw whirling milling, the analysis of cutting temperature is different from turning or milling due to the complicated contact characteristics between the tool, workpiece and chip. In this study, a temperature model is developed for predicting the temperature distribution of the cutting area in screw whirling milling at the two cutting stages. Temperature experiments on the ball screw shaft are carried out in whirling milling machine under different cutting conditions to verify the proposed model. The maximum temperature of the cutting area increases with the cutting speed at first and decreases subsequently. The maximum temperature increases with the rotation of the tool ring and then decreases in one cut.

Keywords: Screw whirling milling, temperature distribution, cutting stage, geometric analysis

1 INTRODUCTION

In the metal cutting process, only 1%-3% of the energy consumed by the machine tool is retained in the system to form a new workpiece surface, and the rest is converted into cutting heat [Sales 2020]. The accumulation of cutting heat will lead to the rapid increase of cutting temperature in the cutting area, which will accelerate the softening and wear of tools, thus reducing the service life of tools [Cui 2017]. As a dry cutting technique (without lubricant), whirling milling is a fast method of machining of the screw compared to milling [Mohan 2007]. Whirling milling can better meet the production requirements and ecological requirements of machining of the screw. In the cutting process of screw whirling milling, cutting temperature is inevitable at the cutting area which significantly affects the operational performance of the workpiece in the use phase of the product. To improve the operational performance of the workpiece, temperature analysis of the cutting area in screw whirling milling is worth to investigate during the manufacturing phase of the product.

Most of the research on temperature analysis is focused on continuous cutting. Komanduri and Hou [Komanduri 2000, 2001] gave a comprehensive review of the state-of-the-art in analytical methods to estimate the temperature in the cutting area for turning. Following the analysis of Komanduri and Hou, Artozoul et al. [Artozoul 2015] proposed a parametric model for the heat source representing the secondary shear zone to determine the temperature distribution in the tool and the work material during an orthogonal cutting process. Considering the cooling procedure of the workpiece, Huang and Wang

[Huang 2016] improved the model proposed by Komanduri and Hou by introducing the heating time at the point of interest in the workpiece to estimate the workpiece temperature in orthogonal cutting. As a kind of interrupted cutting technology, screw whirling milling is much different from the continuous cutting process in the aspect of temperature analysis.

According to Abukhshim et al. [Abukhshim 2006], the thermal state in the interrupted cutting process (such as milling) is different from those in the continuous cutting process (such as turning). To understand the mechanism of heat generation, prediction and analysis of temperature distribution in the interrupted cutting processes have attracted great interest of scholars. Both Sato et al [Sato 2011] and Karaguzel et al. [Karaguzel 2016] employed a Green's function approach to predict the temperature variation of the cutting tool in milling. They concluded that the area, intensity, and duration of the heat source were the main factors that affect the tool temperature. Cui et al. [Cui 2012] proposed a theoretical thermal model to calculate and analyze the transient average tool temperatures in face milling. The study established an analytical model for the tool temperature with the consideration of the variation of heat source induced by the un-deformed chip thickness. In addition, Kuo et al. [Kuo 2012] presented a temperature model to calculate the transient temperature of the milling tool. The analysis of the transient tool temperature was based on the time-dependent heat source and the time-varying tool-chip contact zone induced by the un-deformed chip thickness. However, the time-varying of the uncut chip width has not been considered in the above models. In screw whirling milling, the tool trajectory relative to the

workpiece is complicated which induces a transient change of the uncut chip geometry and tool-chip contact condition. Therefore, a new temperature model which is suitable for screw whirling milling need to be developed.

In this paper, a temperature model of screw whirling milling in the manufacturing phase of the product is developed for predicting the temperature distribution in the cutting area. The geometric analysis from the aspects of the uncut chip geometry and tool-chip contact condition at the two cutting stages is presented as the input parameters of the temperature model. A series of experiments have been conducted to verify the proposed model. In addition, the effect of cutting speed on the temperature distribution of the workpiece, chip and tool are analyzed to illuminate the instantaneous characteristics of the temperature.

2 GEOMETRIC ANALYSIS FOR SCREW WHIRLING MILLING

In screw whirling milling, a series of tool tips remove material by passing over the rotating workpiece and advancing at lead to produce a helical form [Lee 2008]. Fig. 1 is the schematic diagram of screw whirling, and the whirling process includes four types of motion. These are the rotation of the workpiece, the rotation of the tool ring, the axial translation of the tool and the radial translation of the tool.
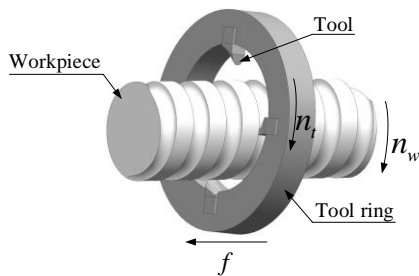
Fig. 1: Schematic diagram of screw whirling milling.

To evaluate the temperature distributions in the workpiece, chip and tool for screw whirling milling, the geometric analysis from the aspects of the uncut chip geometry and tool-chip contact condition is needed. According to the cutting mechanism of screw whirling milling, the cutting process can be divided into two cutting stages to better understand the geometrical characteristics of the cutting process.

2.1 Definition of uncut chip geometry

The uncut chip geometry including thickness, width and area are the input parameters of the temperature model for workpiece and chip. The schematic diagram of the uncut chip geometry for the $(n+1)$-th tool in the two cutting stages is shown in Fig. 2. In Fig. 2, r and R are the outer diameter of the screw and the tool tip turning radius, respectively; e, θ and Δ are the eccentric offset distance between the workpiece center and tool trajectory center, the rotation angle of the $(n+1)$-th tool ring and the angle of the tool initially cuts into the workpiece, respectively; the point $P1$ $(y_1(\Delta+\theta)$, $z_1(\Delta+\theta))$ to $P5$ $(y_5(\Delta+\theta)$, $z_5(\Delta+\theta))$ are the intersection of the guideline (line l_n and line l_{n+1}) between the outer diameter of the workpiece and the tool trajectory.

According to the analysis of the complex relative trajectories between the workpiece and tool, the uncut chip thickness, width and area are analyzed. In addition, the input parameters ($\rho_{x(n)}$ and $\rho_{x(n+1)}$) for the uncut chip geometry have also been formulated. The detailed equations of the uncut chip geometry and the input parameters are presented in Table 1.

Tab. 1: Formulation of uncut chip geometry.

Descriptions	Equations	
First cutting stage		
Uncut chip thickness	$H_1(\theta) = \sqrt{\begin{array}{c}(y_1(\Delta+\theta) - y_2(\Delta+\theta))^2 + \\ (z_1(\Delta+\theta) - z_2(\Delta+\theta))^2\end{array}}$	(1)
Uncut chip width for $(n+1)$-th tool	$w_1 = 2r_{tool}\sin(\rho_{x(n+1)}/2)$	(2)
Uncut chip width for n-th tool	$w' = 2r_{tool}\sin(\rho_{x(n)}/2)$	(3)
Uncut chip area	$S_1(\theta) = \dfrac{1}{2}r_{tool}^2(\rho_{x(n+1)} - \sin\rho_{x(n+1)})$	(4)
Second cutting stage		
Uncut chip thickness	$H_3(\theta) = \sqrt{\begin{array}{c}(y_3(\Delta+\theta) - y_2(\Delta+\theta))^2 + \\ (z_3(\Delta+\theta) - z_2(\Delta+\theta))^2\end{array}}$	(5)
Uncut chip area	$S_2(\theta) = 1/2\, r_{tool}^2(\rho_{x(n+1)} - \sin\rho_{x(n+1)})$ $- 1/2\, r_{tool}^2(\rho_{x(n)} - \sin\rho_{x(n)})$	(6)
Input parameters		
	$\rho_{x(n)} = 2\arccos((r_{tool} - H_2(\theta))/r_{tool})$	(7)
	$\rho_{x(n+1)} = 2\arccos((r_{tool} - H_1(\theta))/r_{tool})$	(8)
	$H_2(\theta) = \sqrt{\begin{array}{c}(y_5(\Delta+\theta) - y_4(\Delta+\theta))^2 + \\ (z_5(\Delta+\theta) - z_4(\Delta+\theta))^2\end{array}}$	(9)

2.2 Definition of tool-chip contact condition

The tool-chip contact condition has an impact on the frictional heat source in the tool-chip interface which further affects the temperature distribution of the tool. A single circular arc tool was adopted in this paper, and the tool-chip contact area for screw whirling milling in the two cutting stages is shown in Fig. 3. In Fig. 3, r_{tool} is the outer diameter of the tool; $\rho_{x(n)}$ and $\rho_{x(n+1)}$ are center angle corresponding to the tool's circular profile inserting the workpiece in the two cutting stages; δ_1, δ_2 and δ_3 are the tool center angle corresponding to the first, second and third section in the second cutting stages; $f_1(x, y)$ to $f_6(x, y)$ and $f_1'(x, y)$ to $f_6'(x, y)$ are the boundary equations of the frictional heat source area.
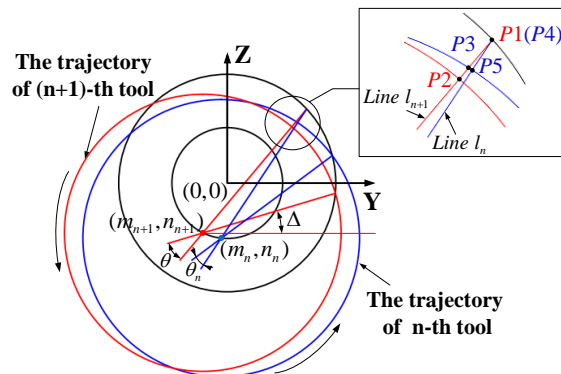
Fig. 2: The variation of the uncut chip geometry in the two cutting stages.
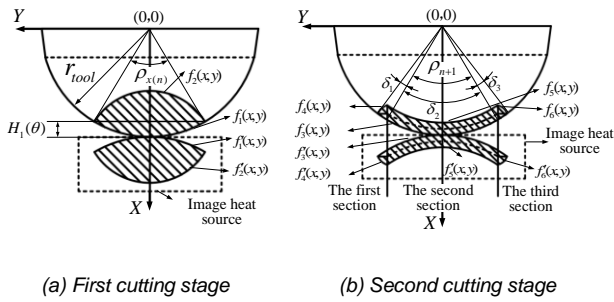
(a) First cutting stage   (b) Second cutting stage

Fig. 3: Contact analysis of the tool and chip in the two cutting stages.

Based on the contact analysis of the tool and chip, the detailed boundary equations of the frictional heat source are presented in Table 2.

Tab. 2: Formulation of boundary equations.

Descriptions	Equations
First cutting stage	

$$f_1(x, y) = \sqrt{r_{tool}^2 - y^2} \quad (10)$$

$$f_2(x, y) = \sqrt{r_{tool}^2 - y^2} - 2\left(\begin{array}{c} r_{tool}\cos\delta - \\ r_{tool} + H_1(\theta) \end{array} \right) \quad (11)$$
$$\cos(\phi - \alpha)/\sin\phi$$

$$f_1'(x, y) = -\sqrt{r_{tool}^2 - y^2} + 2r_{tool} \quad (12)$$

$$f_2'(x, y) = -\sqrt{r_{tool}^2 - y^2} + 2\left(\begin{array}{c} r_{tool}\cos\delta - \\ r_{tool} + H_1(\theta) \end{array} \right) \quad (13)$$
$$\cos(\phi - \alpha)/\sin\phi + 2r_{tool}$$

Second cutting stage

$$f_3(x, y) = \sqrt{r_{tool}^2 - y^2} \quad (14)$$

$$f_4(x, y) = \sqrt{r_{tool}^2 - y^2} - 2\left(\begin{array}{c} \sqrt{r_{tool}^2 - y^2} - \\ r_{tool}\cos\dfrac{\rho_{x(n+1)}}{2} \end{array} \right) \quad (15)$$
$$\cos(\phi - \alpha)/\sin\phi$$

$$f_5(x, y) = \sqrt{r_{tool}^2 - y^2} - 2H_3(\theta) \quad (16)$$
$$\cos(\phi - \alpha)/\sin\phi$$

$$f_6(x, y) = \sqrt{r_{tool}^2 - y^2} - 2\left(\begin{array}{c} \sqrt{r_{tool}^2 - y^2} - \\ r_{tool}\cos\dfrac{\rho_{x(n+1)}}{2} \end{array} \right) \quad (17)$$
$$\cos(\phi - \alpha)/\sin\phi$$

$$f_3'(x, y) = -\sqrt{r_{tool}^2 - y^2} + 2r_{tool} \quad (18)$$

$$f_4'(x, y) = -\sqrt{r_{tool}^2 - y^2} + 2\left(\begin{array}{c} \sqrt{r_{tool}^2 - y^2} - \\ r_{tool}\cos\dfrac{\rho_{x(n+1)}}{2} \end{array} \right) \quad (19)$$
$$\cos(\phi - \alpha)/\sin\phi + 2r_{tool}$$

$$f_5'(x, y) = -\sqrt{r_{tool}^2 - y^2} + 2H_3(\theta) \quad (20)$$
$$\cos(\phi - \alpha)/\sin\phi + 2r_{tool}$$

$$f_6'(x, y) = -\sqrt{r_{tool}^2 - y^2} + 2\left(\begin{array}{c} \sqrt{r_{tool}^2 - y^2} - \\ r_{tool}\cos\dfrac{\rho_{x(n+1)}}{2} \end{array} \right) \quad (21)$$
$$\cos(\phi - \alpha)/\sin\phi + 2r_{tool}$$

3 CUTTING TEMPERATURE MODEL FOR SCREW WHIRLING MILLING

In general, the modeling concept proposed is based on the well-known principle of the simultaneous action of two independent heat sources (the shear plane heat source in primary deformation and the frictional heat source in secondary deformation) [Shaw 1989]. The heat generation is affected by three regions: primary deformation zone in the shear plane, secondary deformation zone in the tool-chip interface and tertiary deformation zone in the tool-workpiece interface (as shown in Fig. 4). Tertiary deformation zone occurs at the rubbing contact between the tool flank face and the newly machined surface of the workpiece [Abukhshim 2005]. The contribution of tertiary deformation zone does not make a significant difference in the temperature rise, and hence the influences of tertiary deformation zone on the temperature in the cutting field can be ignored [Abukhshim 2006]. Based on the research of Komanduri and Hou [Komanduri 2000, 2001], the temperature models for the workpiece, chip and tool are developed at the two cutting stages in this section.
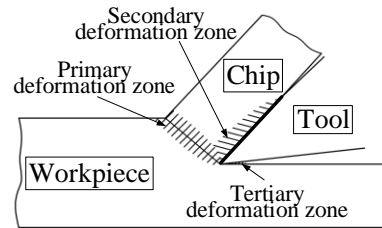
Fig. 4: Heat generation occurs in cutting zone.

3.1 Workpiece temperature model

The temperature rise of the workpiece is mainly caused by the shear plane heat source in the primary deformation. The time-varying temperature rise model $\theta_{workpiece}$ for workpiece induced by the shear plane heat source is constructed in the following.

$$\theta_{workpiece} = \frac{q_s}{2\pi\lambda_w} \int_{l_i=0}^{L} e^{-(X - l_i \sin\varphi)V_s/2a}$$
$$\left\{ K_o\left[\frac{V_s}{2a}\sqrt{(X - l_i\sin\varphi)^2 + (Z - l_i\cos\varphi)^2} \right] + \right.$$
$$\left. K_o\left[\frac{V_s}{2a}\sqrt{(X - l_i\sin\varphi)^2 + (Z + l_i\cos\varphi)^2} \right] \right\} dl_i \quad (22)$$

where λ_w is the thermal conductivity of the workpiece; L is the width of the heat source; l_i is the location of the differential small segment of the shear band heat source; φ, V_s, a and K_0 are the oblique angle, shear velocity, thermal diffusivity and zero-order Bessel function, respectively; X and Z are the coordinates of the interesting point in the workpiece; q_s is the heat liberation intensity for the workpiece and it can be derived as [Chou 2003]:

$$q_s = F_s V_s / A_s \quad (23)$$

where V_s can be expressed by $V_s=V\cos\alpha/\cos(\phi-\alpha)$ [Karpat 2006]; A_s and L are the area and width of the shear plane heat source and they can be obtained from Section 2.

$$A_s = \begin{cases} S_1(\theta)/\sin\phi, & first\ cutting\ stage \\ S_2(\theta)/\sin\phi, & sec\,ond\ cutting\ stage \end{cases}$$

(24)

$$L = \begin{cases} H_1(\theta)/\sin\phi, & first\ cutting\ stage \\ H_3(\theta)/\sin\phi, & sec\,ond\ cutting\ stage \end{cases}$$

(25)

3.2 Chip temperature model

The temperature rise of the chip is mainly caused by the shear plane heat source and the frictional heat source. The time-varying temperature rise model $\theta_{chip-shear}$ for chip induced by the shear plane heat source is constructed in the following.

$$\theta_{chip-shear} = \frac{q_s}{2\pi\lambda_t} \int_{w_i=0}^{t_{ch}/\cos(\phi-\alpha)} e^{-(X-X_i)V_s/2a}$$
$$\left\{ K_o\left[\frac{V_s}{2a}\sqrt{\begin{array}{l}(X-(r_{tool}-w_i\sin(\phi-\alpha)))^2 + \\ (Z-w_i\cos(\phi-\alpha))^2\end{array}}\right] + \right.$$
$$\left. K_o\left[\frac{V_s}{2a}\sqrt{\begin{array}{l}(X-(r_{tool}-w_i\sin(\phi-\alpha)))^2 + \\ (2t_{ch}-Z-w_i\cos(\phi-\alpha))^2\end{array}}\right] \right\} dw_i$$

(26)

where λ_t and r_{tool} are the thermal conductivity and outer diameter of the tool; t_{ch} is the chip thickness, and it can be given as $t_{ch}=t_c\cos(\phi-\alpha)/\sin\phi$ [Toropov 2003]; q_s is the heat liberation intensity of shear plane heat source, and it can be derived by Equation (22).

The time-varying temperature rise model $\theta_{chip-frictional}$ for chip induced by the frictional heat source is constructed in the following.

$$\theta_{chip-frictional} = \frac{q_r B_{chip}}{\pi\lambda_t} \int_{r_{tool}}^{r_{tool}-L'} e^{-(X-l_i-(r_{tool}-L'))V_c/2a}$$
$$\left[K_0\left(R_{chip}V_{ch}/2a\right) + K_0\left(R'_{chip}V_{ch}/2a\right) \right] dl_i$$

(27)

where B_{chip} is the fraction of the heat conducted into the chip which could be obtained by the research of [Komanduri 2000]; $R_{chip} = \sqrt{(X-l_i-r_{tool})^2 + z^2}$, $R'_{chip} = \sqrt{(X-l_i-r_{tool})^2 + (2t_{ch}-z)^2}$; q_r is the heat liberation intensity of frictional heat source and it can be illustrated as [Chou 2003]:

$$q_r = F_f V_{ch}/A_r$$

(28)

where V_{ch} is chip velocity, and it can be expressed by $V_{ch}=V\sin\phi/\cos(\phi-\alpha)$ [Karpat 2006]; A_r and L' are the area and length of frictional heat source, respectively, and they can be illustrated from Section 2.

$$A_r = \begin{cases} \int_{\delta_{11}}^{\delta_{12}} w\cdot L_c(\delta)\,d\delta, & first\ cutting\ stage \\ \int_{\delta_{11}}^{\delta_{12}} w\cdot L_c(\delta)\,d\delta - \\ \int_{\delta_{11}'}^{\delta_{22}'} w'\cdot L_c'(\delta)\,d\delta', & sec\,ond\ cutting\ stage \end{cases}$$

(29)

$$L' = \begin{cases} 2H_1(\theta)\cos(\phi-\alpha)/\sin\phi & first\ cutting\ stage \\ 2H_3(\theta)\cos(\phi-\alpha)/\sin\phi & sec\,ond\ cutting\ stage \end{cases}$$

(30)

where δ_{11} and δ_{12} are the (n+1)-th tool center angle corresponding to the cutting edge in the first-cutting stage, δ'_{11} and δ'_{12} are the n-th tool center angle corresponding to the cutting edge in second-cutting stage of the (n+1)-th tool.

According to the comprehensive effect of the shear plane heat source and frictional heat source on the temperature rise of the chip, the chip temperature rise θ_{chip} can be obtained.

3.3 Tool temperature model

The temperature rise in the tool mainly caused by the heat generation in the frictional heat source. The temperature rise θ_{tool-1} at any point in the tool caused by the frictional heat source in the stage of first-cutting is given by the following.

$$\theta_{tool-1} = \frac{q_r B_{tool}}{2\pi\lambda_t} \int_{-r_{tool}\sin\frac{\rho_{n+1}}{2}}^{r_{tool}\sin\frac{\rho_{n+1}}{2}} \left[\int_{f_2(x,y)}^{f_1(x,y)} \left(1/R_{tool}\right) dx_i + \int_{f_2'(x,y)}^{f_1'(x,y)} \left(1/R'_{tool}\right) dx_i \right] dy_i$$

(31)

The temperature rise θ_{tool-2} of three sections at any point in the tool caused by the frictional heat source in the stage of second-cutting is given by the following.

$$\theta_{tool-2} = \begin{cases} \frac{q_r B_{tool}}{2\pi\lambda_t} \int_{\sqrt{r_{tool}^2 - \left(r_{tool}\cos\frac{\rho_{n+1}}{2}+H_3(\theta)\right)^2}}^{r_{tool}\sin\frac{\rho_{n+1}}{2}} \left[\int_{f_4(x,y)}^{f_3(x,y)}\left(1/R_{tool}\right)dx_i + \int_{f_3'(x,y)}^{f_4'(x,y)}\left(1/R'_{tool}\right)dx_i \right] dy_i \\ \frac{q_r B_{tool}}{2\pi\lambda_t} \int_{-\sqrt{r_{tool}^2 - \left(r_{tool}\cos\frac{\rho_{n+1}}{2}+H_3(\theta)\right)^2}}^{\sqrt{r_{tool}^2 - \left(r_{tool}\cos\frac{\rho_{n+1}}{2}+H_3(\theta)\right)^2}} \left[\int_{f_5(x,y)}^{f_3(x,y)}\left(1/R_{tool}\right)dx_i + \int_{f_3'(x,y)}^{f_5'(x,y)}\left(1/R'_{tool}\right)dx_i \right] dy_i \\ \frac{q_r B_{tool}}{2\pi\lambda_t} \int_{-r_{tool}\sin\frac{\rho_{n+1}}{2}}^{-\sqrt{r_{tool}^2 - \left(r_{tool}\cos\frac{\rho_{n+1}}{2}+H_3(\theta)\right)^2}} \left[\int_{f_6(x,y)}^{f_3(x,y)}\left(1/R_{tool}\right)dx_i + \int_{f_3'(x,y)}^{f_6'(x,y)}\left(1/R'_{tool}\right)dx_i \right] dy_i \end{cases}$$

(32)

where B_{tool} is the fraction of the heat conducted into the tool which can be obtained by the literature of [Komanduri 2000]; $R_{tool} = \sqrt{(x-x_i)^2 + (y-y_i)^2 + z^2}$, $R'_{tool} = \sqrt{(x-2r_{tool}+x_i)^2 + (y-y_i)^2 + z^2}$.

4 EXPERIMENTAL VALIDATION AND DISCUSSION

Experiments on the ball screw shaft for different cutting conditions were conducted on CNC whirling milling machine to verify the temperature model. The cutting force data as the input parameters of the temperature model was obtained by experiment and it was collected by Kistler dynamometer shown in Fig. 5. Due to the complexity of the process of screw whirling milling, it is difficult to obtain the temperature of the cutting area by contact temperature measurement. During the experiments, therefore, the temperature was indirectly measured through non-contact infrared thermal imaging which was offered by FLIR. Fig. 6 is the maximum temperature of the cutting area at some

point in the cutting process collected by infrared thermal imaging. In the experiment, the material of the tool and the workpiece of the screw were PCBN and AISI 52100, respectively. The geometrical and thermophysical parameters of the tool and workpiece in the temperature model can be summarized in Table 3.
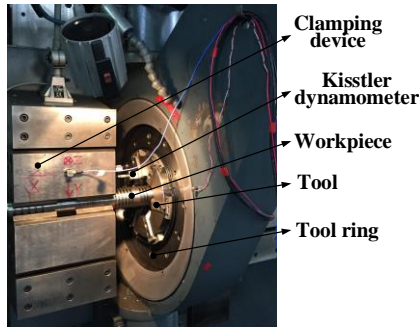
Fig. 5 : Experimental setup.
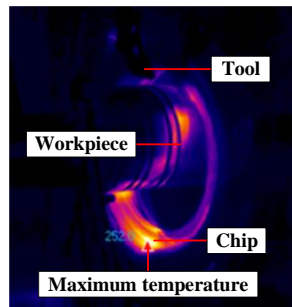
Fig. 6: The temperature value of the cutting process collected by FLIR.

Tab. 3: Values of the geometrical and thermophysical parameters of the tool and workpiece.

Tool values		Workpiece values	
Rake angle	0°	Outer diameter of screw	7.85 cm
Nose radius	0.366 cm	Root diameter of screw	7.39 cm
Thermal conductivity	0.44 W/(cm ℃)	Thermal conductivity	0.466 W/(cm ℃)
Specific heat	0.75 J/(g ℃)	Thermal diffusivity	0.126 cm2/s
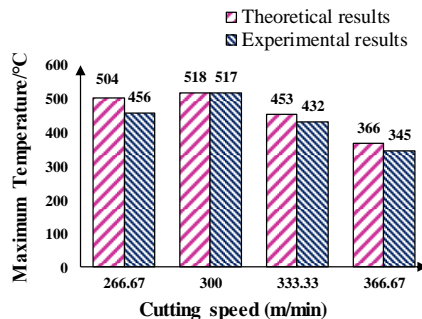
Fig. 7: Temperature values of measurements and prediction.

The temperature model simulations and the experimental tests were performed at the cutting speed of 160 m/min, 180 m/min, 200 m/min and 220 m/min with 4 tools. The other cutting parameters such as depth of cut and feed rate of the tool ring are changing with the selection of the cutting speed. In the calculation of the temperature,

one thousand target points were selected in the workpiece surface (in the area of 0.3 cm × 0.3 cm), chip surface (in the area of 0.3 cm × 0.3 cm) and tool surface (in the area of 0.3 cm × 0.3 cm) to acquire the maximum temperature. The temperature values of the experimental and theoretical are shown in Fig. 7. The experimental results show to be consistent well with the theoretical results, and the theoretical results obtained by the proposed model are slightly larger than the experimental values. It should be noted out that the cutting temperature increases with the cutting speed at first and decreases subsequently. The phenomenon of cutting temperature changing with cutting speed is consistent with Salomon's hypothesis. This is because during high speed cutting, the thermal effect reduces the strength and shear stress of the material, causing it to soften. Therefore, during high speed cutting, the required cutting force is reduced, and the heat generated in the cutting area is small, resulting in a decrease in cutting temperature.

In screw whirling milling, the temperature distribution is instantaneous in the two cutting stages. The instantaneous characteristic can be illuminated by taking the temperature distribution at the cutting speed of 160 m/min as an example, shown in Fig. 8. In Fig. 8, the maximum temperature of the cutting area increases at the first cutting stage and then decreases at the second cutting stage. The chip temperature rapid increases and then decreases slowly; the workpiece temperature rapid increases and then remain little changes; the tool temperature changes little. The tool temperature is smaller than the chip and the workpiece temperature. The chip temperature is higher than the workpiece temperature during the first 1/2 stage of the one cut. During the last 1/2 stage of the one cut, the chip temperature is smaller than the workpiece temperature. The maximum temperature occurs at the chip and then occurs at the workpiece as the rotation of the cutter head, and the maximum temperature of the cutting area appears in the chip during one cut.
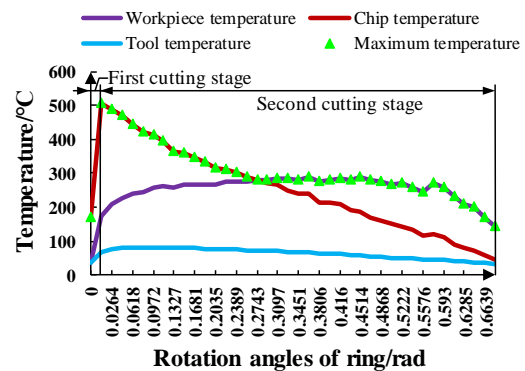
Fig. 8: Temperature distribution at the cutting speed of 160 m/min.

5 CONCLUSIONS

In this paper, a temperature model is developed for predicting the temperature distribution of the cutting area during the manufacturing phase of the product for screw whirling milling. The geometric analysis of the uncut chip and tool-chip contact condition at the two cutting stages are added to the temperature model. The theoretical results of the temperature obtained by the mathematical thermal model coincided well with the experimental data under different cutting conditions. The maximum temperature of

the cutting area increases with the cutting speed at first and decreases subsequently. The cutting speed of the maximum temperature in the cutting area is 180 m/min under the four cutting conditions. In addition, the maximum temperature increases with the rotation of the tool ring and then decreases in one cut. The demarcation point between first-cutting stage and second-cutting stage is the location of the maximum temperature. The future work will be conducted to analyze the impact of the workpiece temperature on the operational performance of part to improve service life of the workpiece.

6 ACKNOWLEDGMENTS

7 REFERENCES

[Abukhshim 2006] Abukhshim, N. A., et al. Heat generation and temperature prediction in metal cutting: A review and implications for high speed machining. International Journal of Machine Tools and Manufacture, 2006, 46(7-8), 782-800. 0890-6955

[Abukhshim 2005] Abukhshim, N. A., et al. Investigation of heat partition in high speed turning of high strength alloy steel. International Journal of Machine Tools and Manufacture, 2005, 45(15), 1687-1695. 0890-6955

[Artozoul 2015] Artozoul, J., et al. Experimental and analytical combined thermal approach for local tribological understanding in metal cutting. Applied Thermal Engineering, 2015, 89, 394-404. 1359-4311

[Chou 2003] Chou, Y. K., Song, H. Thermal modeling for hard turning using a new tool. International Mechanical Engineering Congress and Exposition, 2003, 183-192.

[Cui 2017] Cui, X. and Guo, J. Effects of cutting parameters on tool temperatures in intermittent turning with the formation of serrated chip considered. Applied Thermal Engineering, 2017, 110, 1220-1229. 1359-4311

[Cui 2012] Cui, X., et al. Analysis of transient average tool temperatures in face milling. International Communications in Heat and Mass Transfer, 2012, 39(6), 786-791. 0735-1933

[Huang 2016] Huang, K. and Yang, W. Analytical model of temperature field in workpiece machined surface layer in orthogonal cutting. Journal of Materials Processing Technology, 2016, 229, 375-389. 0924-0136

[Karaguzel 2016] Karaguzel, U., et al. Modeling and Measurement of Cutting Temperatures in Milling. Procedia CIRP, 2016, 173-176.

[Karpat 2006] Karpat, Y., Özel, T. Predictive Analytical and Thermal Modeling of Orthogonal Cutting Process-Part I: Predictions of Tool Forces, Stresses, and Temperature Distributions. Journal of Manufacturing Science and Engineering-Transactions of the ASME, 2006, 128(2), 33-6. 1087-1357

[Komanduri 2001] Komanduri, R. and Hou, Z. B. Thermal modeling of the metal cutting process Part II-Temperature rise distribution due to frictional heat source at the tool-chip interface. International Journal of Mechanical Sciences, 2001, 43(1), 57-88. 0020-7403

[Komanduri 2001] Komanduri, R. and Hou, Z. B. Thermal modeling of the metal cutting process Part III-Temperature rise distribution due to the combined effects of shear plane heat source and the tool-chip interface frictional heat source. International Journal of Mechanical Sciences, 2001, 43(1), 89-107. 0020-7403

[Komanduri 2000] Komanduri, R. and Hou, Z. B. Thermal modeling of the metal cutting process Part I-Temperature rise distribution due to shear plane heat source. International Journal of Mechanical Sciences, 2000, 42(9), 1715-1752. 0020-7403

[Kuo 2012] Kuo, H. Y, et al. Estimation of milling tool temperature considering coolant and wear. Journal of Manufacturing Science and Engineering-Transactions of the ASME, 2012, 134(3), 031002. 1087-1357

[Lee 2008] Lee, M. H., et al. Investigation of cutting characteristics for worm machining on automatic lathe - Comparison of planetary milling and side milling. Journal of Mechanical Science and Technology, 2008, 22(12), 2454-2463. 1738-494X

[Mohan 2007] Mohan, L. V. and Shunmugam, M. S. Simulation of whirling process and tool profiling for machining of worms. Journal of Materials Processing Technology, 2007, 185(1), 191-197. 0924-0136

[Sales 2020] Sales, W. F., et al. A review of surface integrity in machining of hardened steels. Journal of Manufacturing Processes, 2020, 58, 136-162. 1526-6125

[Sato 2011] Sato, M., et al. Temperature Variation in the Cutting Tool in End Milling. Journal of Manufacturing Science and Engineering-Transactions of the ASME, 2011, 133(2), 021005. 1087-1357

[Shaw 1989] Shaw, M. C. Metal Cutting Principles. Clarendon Press, Oxford, 1989.

[Toropov 2003] Toropov, A., Ko. S. L. Prediction of tool-chip contact length using a new slip-line solution for orthogonal cutting. International Journal of Machine Tools and Manufacture, 2003, 43(12), 1209-1215. 0890-695